

# Discovering Higgs Bosons of the MSSM using Jet Substructure

Graham D. Kribs,<sup>1</sup> Adam Martin,<sup>2</sup> Tuhin S. Roy,<sup>1</sup> and Michael Spannowsky<sup>1</sup>

<sup>1</sup>*Department of Physics, University of Oregon, Eugene, OR 97403*

<sup>2</sup>*Theoretical Physics Department, Fermilab, Batavia, IL 60510*

We present a qualitatively new approach to discover Higgs bosons of the MSSM at the LHC using jet substructure techniques applied to boosted Higgs decays. These techniques are ideally suited to the MSSM, since the lightest Higgs boson overwhelmingly decays to  $b\bar{b}$  throughout the entire parameter space, while the heavier neutral Higgs bosons, if light enough to be produced in a cascade, also predominantly decay to  $b\bar{b}$ . The Higgs production we consider arises from superpartner production where superpartners cascade decay into Higgs bosons. We study this mode of Higgs production for several superpartner hierarchies:  $m_{\tilde{q}}, m_{\tilde{g}} > m_{\tilde{W}, \tilde{B}} > m_h + \mu$ ;  $m_{\tilde{q}}, m_{\tilde{g}} > m_{\tilde{W}, \tilde{B}} > m_{h, H, A} + \mu$ ; and  $m_{\tilde{q}}, m_{\tilde{g}} > m_{\tilde{W}} > m_h + \mu$  with  $m_{\tilde{B}} \simeq \mu$ . In these cascades, the Higgs bosons are boosted, with  $p_T > 200$  GeV a large fraction of the time. Since Higgses appear in cascades originating from squarks and/or gluinos, the cross section for *events with at least one Higgs* can be the same order as squark/gluino production. Given  $10 \text{ fb}^{-1}$  of 14 TeV LHC data, with  $m_{\tilde{q}} \lesssim 1$  TeV, and one of the above superpartner mass hierarchies, our estimate of  $S/\sqrt{B}$  of the Higgs signal is sufficiently high that the  $b\bar{b}$  mode can become *the* discovery mode of the lightest Higgs boson of the MSSM.

## I. INTRODUCTION

Uncovering the origin of electroweak symmetry breaking is of the utmost importance for the LHC. If the world is supersymmetric – in the form of the minimal supersymmetric standard model (MSSM) – electroweak symmetry breaking is accomplished through a supersymmetrized two-Higgs-doublet model, with couplings and interactions set or restricted by supersymmetry.

It is well known that imposing the proper electroweak symmetry breaking minimum leaves two undetermined parameters in the Higgs sector at tree-level: the ratio of the Higgs scalar vevs,  $\tan \beta$ , and the mass of the CP-odd scalar,  $m_A$ . Radiative corrections dominantly affect the lightest Higgs mass, raising it from the ruled-out tree-level value  $m_h = M_Z$  up to about 125 GeV for stop masses and mixings that do not exceed 1 TeV [1]. Decay rates of the Higgs bosons can also be computed largely independently of the details of the superpartner sector (so long as decays into superpartners are either kinematically forbidden or rarely occur). The Higgs sector can thus seemingly be approximately parametrized by  $m_h, m_A, \tan \beta$ .

This has reinforced the simplification that the Higgs scalar sector can be searched for, discovered, or ruled out in isolation from the remainder of the model [2]. A casual glance at the ATLAS or CMS TDRs [3, 4] demonstrates this canonical view, in which discovery potential for the Higgs sector is plotted in the  $m_A$ - $\tan \beta$  plane (with some additional restriction on  $m_h$  larger than the LEP II bound). The Achilles heel of this simplification is the assumption that the most promising production channels of the Higgs bosons are largely the same ones as in the Standard Model (SM).

We demonstrate there is potentially a *much superior* way to discover Higgs bosons in the MSSM – superpartner production with superpartners that cascade decay into Higgs bosons. Higgs bosons from superpartner cas-

cades is not a new idea, see e.g. [5–12], but our method for finding and identifying Higgs bosons within the supersymmetric event sample is qualitatively new. We exploit recently developed jet substructure techniques [13] with modifications that we presented in Ref. [14] to isolate the boosted Higgs-to- $b\bar{b}$  signal from the Standard Model and supersymmetric backgrounds. The existence of a large supersymmetric cascade-to-Higgs rate requires relatively mild assumptions about the superpartner mass hierarchy.

The notion to find and study supersymmetric signals through the hadronic decays of gauge bosons, as well as the lightest Higgs boson, was pointed out in an early use of jet substructure in Ref. [15]. There, however, the motivation was *not* to find the Higgs, but instead to recover the superpartner mass spectrum using a kinematical edge analysis.

In our previous paper [14], we pointed out that a signal of the Higgs boson itself can often be much more easily found within new physics, since the new physics can have a larger production cross section and larger fraction of boosted Higgs bosons. But identifying the Higgs boson in processes that invariably have busier final states with more jets (and potentially more hard  $b$ -jets) required modest improvements to the BDRS algorithm. This is not unlike the situation faced by Ref. [16] in proposing a method to extract the Higgs signal from  $t\bar{t}h$  production.

The *commonalities* between our previous work, Ref. [14], and this paper are:

1. We seek two-body decays of a Higgs boson into  $b\bar{b}$ .
2. We use the same jet substructure algorithm to extract this Higgs signal.
3. The Study Points in this paper are pure MSSM.
4. We apply fairly aggressive cuts to reduce the backgrounds from standard model processes.

The main *differences* between Ref. [14] and this paper are:

1. The LSP of the MSSM-based Study Points in this paper is a neutralino<sup>1</sup>. Our previous work, instead considered study points with a gravitino LSP and a promptly decaying Higgsino NLSP.
2. The new physics signal is large missing energy, with characteristically large  $H_T^{\text{jets}}$ . (Our previous work, instead considered the new physics signal to be one hard  $\gamma$  plus missing energy.) This means that while the LHC will have evidence for new physics in channels involving large missing energy, it quite unlikely that the new physics signals can be readily identified with specific processes or decays (or models, for that matter).
3. In this paper, we also consider the detection of  $H$  and  $A$  states decaying to  $b\bar{b}$ , using jet substructure techniques. We demonstrate that for lighter  $m_A \lesssim 200$  GeV, it is possible to uncover evidence both *both*  $h$  and  $H/A$  with just  $10 \text{ fb}^{-1}$  of data.

The organization of the paper is as follows: In Sec. II we explain how Higgs bosons can be produced from specific kinds of two-body superpartner decays. The main emphasis is on the qualitative features of gaugino and Higgsino interactions, so as to present a very clear picture of what superpartner hierarchies provide the most promising source of Higgs bosons, and how the large rates can be easily understood. In Sec. III we consider the typically largest production source of heavy gauginos, namely, squark production and decay into gauginos. We clearly demarcate which superpartners decay into which gauginos, so that further studies can be guided by these basic observations. We then consider, for specific hierarchies, the prospect of finding a boosted Higgs in one of these supersymmetric cascades. We show that in a considerable region of the supersymmetric parameter space, as many as one in four typical decay chains originating in a squark and ending in the LSP can contain a significantly boosted Higgs boson. In Sec. IV we show that the supersymmetric parameter space we consider naturally satisfies the upper bounds on the thermal relic density. Moreover, we demonstrate how simple changes in the gaugino mass hierarchy (lowering  $M_1$ ) can result in matching the cosmological density, but without significantly affecting the Higgs boson signal. In Sec. V we then discuss the techniques and algorithm to find Higgs decay using jet substructure. We compare and contrast our methodology with what has been used before for Standard Model production of a Standard Model Higgs boson. In Sec. VI we present a series of Study Points that demonstrate the effectiveness of our algorithm in finding one or more Higgs bosons of the MSSM. The series of plots of

candidate resonance jet mass are the main results of this paper – demonstrating that the  $b\bar{b}$  mode could well be the discovery mode of Higgs bosons at the LHC. Finally, in Sec. VII we conclude with a discussion of our results.

## II. HIGGS FROM SUPERPARTNER DECAY: “GOLDSTONE REGION”

The main focus of the paper is on Higgs bosons that arise from the two-body decays of neutralinos and charginos,

$$\chi_i^0 \rightarrow h/H/A + \chi_j^0 \quad (1)$$

$$\chi_i^\pm \rightarrow h/H/A + \chi_j^\pm. \quad (2)$$

It is instructive to review how these decays come about, and why the decay rate to Higgs bosons can be sizeable throughout the kinematically allowed parameter space.

The centrally important gaugino-Higgs interactions are the kinetic terms of the Higgs supermultiplets. They lead to the component interaction terms [17]

$$\begin{aligned} & -D_\mu H_u^\dagger D^\mu H_u - i\tilde{H}_u \not{D} \tilde{H}_u \\ & -\sqrt{2}g' Y_{H_u} \tilde{B} \tilde{H}_u H_u^* - \sqrt{2}g \tilde{W}^a \tilde{H}_u t^a H_u^* + (u \leftrightarrow d), \end{aligned} \quad (3)$$

where  $Y_{H_u}$  is the hypercharge of the Higgs field. The first term leads to ordinary gauge boson interactions with the Higgs scalars,

$$\begin{aligned} & -(g')^2 B_\mu B^\mu Y_{H_u}^2 H_u^\dagger H_u - g^2 W_\mu^a W^{b\mu} \text{tr}(t^a H_u^\dagger t^b H_u) \\ & +(u \leftrightarrow d) \end{aligned} \quad (4)$$

The second term leads to ordinary gauge boson interactions with the Higgsinos,

$$g' Y_{H_u} B_\mu \tilde{H}_u \sigma^\mu \tilde{H}_u + g W_\mu^a \tilde{H}_u t^a \sigma^\mu \tilde{H}_u + (u \leftrightarrow d). \quad (5)$$

The latter are exactly the same interactions that Standard Model quark or lepton doublets have with Standard Model gauge bosons. Notice that the interaction involves the entire  $\text{SU}(2)$  doublets  $H_u, H_d$ , and thus, all eight real scalars

$$\text{Re}(H_u^0), \text{Im}(H_u^0), H_u^\pm, \text{Re}(H_d^0), \text{Im}(H_d^0), H_d^\pm. \quad (6)$$

In practice, as is very well known, linear combinations of the above become the physical mass eigenstate Higgs bosons ( $h, H, A, H^\pm$ ) as well as the Goldstone bosons ( $w^\pm, z$ ) associated with the Standard Model gauge bosons  $W^\pm, Z$ . The critical observation is that the “supersymmetrized” interactions,

$$-\sqrt{2}g' \tilde{B} \tilde{H}_u H_u^* - \sqrt{2}g \tilde{W}^a \tilde{H}_u t^a H_u^* + (u \leftrightarrow d), \quad (7)$$

necessarily have gauge coupling strength to all components of both Higgs doublets. This means that, all other things considered equal, decays of  $\tilde{B}/\tilde{W} \rightarrow \tilde{H} + h/H/A/H$

<sup>1</sup> It could also be a “neutralino-equivalent”, where the neutralino is a NLSP and the gravitino is LSP, but the lifetime of the NLSP is sufficiently long that its decays are not observed within the collider detectors.

lead to equal branching ratios into the different components of the doublet. A Higgs scalar, therefore, is just as common as a  $W$  or  $Z$  in this type of cascade decay.

In practice, the gaugino interaction eigenstates mix with the Higgsino interaction eigenstates through the same interactions, Eq. (7), that led to large decay rates of gauginos into physical Higgs bosons. In the mass basis, the decays in Eqs. (1),(2) roughly translate into heavier neutralinos  $\chi_{3,4}^0$  and charginos  $\chi_2^\pm$  decaying into their lighter counterparts  $\chi_{1,2}^0$ ,  $\chi_1^\pm$  and Higgs bosons. The relevant branching ratios are thus  $\chi_{4,3}^0 \rightarrow h/H/A + (\chi_1^0 \text{ or } \chi_2^0)$  and  $\chi_2^\pm \rightarrow h/H/A + \chi_1^\pm$ . The other possible decay  $\chi_2 \rightarrow h + \chi_1$  is mostly kinematically forbidden in the region of our interest.

Another type of cascade decay occurs when the Higgsinos are heavier than the winos and/or bino. This opens up the decay channels  $\tilde{H} \rightarrow h/H/A + \tilde{B}/\tilde{W}$ . This might well provide an interesting source of Higgs bosons given a cascade from third generation squarks to  $\tilde{H}$ . Our preliminary work on this cascade suggests it takes more luminosity than  $10 \text{ fb}^{-1}$  (which is the main focus of this paper), and requires adjustments to the cut-based search strategy to optimize for a signal of third generation squarks.

There are yet other superpartner cascade decays that could also lead to Higgs bosons, such as stop decay  $\tilde{t}_2 \rightarrow \tilde{t}_1 + h/A/H$  [18, 19]. To the extent that this process occurs for the specific points in the MSSM parameter space we present below, it is included in our inclusive analysis. In practice, however, the production cross section of just the heavier stop  $\tilde{t}_2$  is small relative to the large number of other squarks (and gluino), while the branching ratio  $\tilde{t}_2 \rightarrow \tilde{t}_1 h$  is also accidentally small when  $m_{\tilde{Q}_3} = m_{\tilde{t}_R}$  which we take for our Study Points. This implies negligible numbers of lightest Higgs bosons arise from  $\tilde{t}_2$  decay.

Finally, there is an interesting possibility of cascade decays into the charged Higgs  $H^\pm$ . If  $m_{H^\pm} > m_t + m_b$ , the hadronic decay mode  $H^+ \rightarrow t\bar{b}$  often has a large fraction, and thus could be an interesting candidate for jet substructure techniques, utilizing top tagging [16, 21–30] or other novel methods.

### III. CASCADING TO BOOSTED HIGGS BOSONS

The largest rate for Higgs boson production arises when first or second generation squarks cascade decay through gauginos, which then decay into lighter Higgsinos and Higgs bosons. Generally, first and second generation squarks decay as

$$\tilde{q}_L \rightarrow q + \tilde{W} \quad (8)$$

$$\tilde{q}_R \rightarrow q + \tilde{B} \quad (9)$$

so long as the wino and bino satisfy the simple kinematical requirement that they are lighter than the squarks. The left-handed squarks can also decay to the bino, but

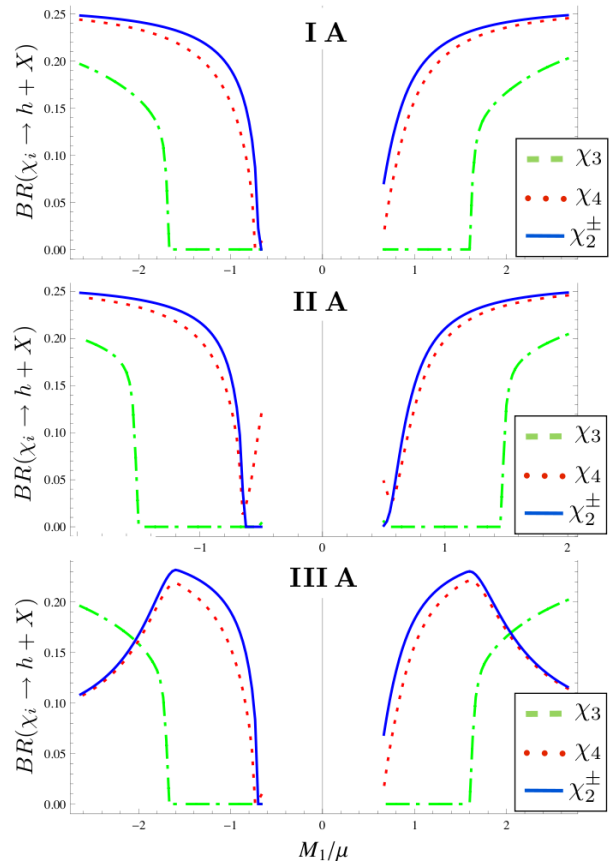


FIG. 1. The branching ratios of heavier gaugino-like neutralinos and charginos into lighter Higgsino-like ones plus the lightest Higgs boson is shown for the following parameters: We take  $100 \text{ GeV} < M_1 = M_2/2 < 400 \text{ GeV}$  for all Figures,  $|\mu| = 150 \text{ GeV}$  in plots I and III and  $|\mu| = 200 \text{ GeV}$  in plots II. Plots I and II have heavier sleptons,  $m_{\tilde{l}} > 800 \text{ GeV}$ , so that two-body decays are kinematically forbidden. In plot III, we take  $m_{\tilde{l}} = 500 \text{ GeV}$ , which allows the wino to decay to left-handed sleptons once  $M_2 > 500 \text{ GeV}$ . This is why the branching ratios of  $\chi_4^0$ ,  $\chi_2^\pm$  decrease above  $M_1/|\mu| > 1.7$ .

this rarely happens when the wino mode is kinematically open, since the ratio of bino to wino couplings for the left-handed squark doublet is proportional to  $Y_Q^2(g'/g)^2 \simeq 0.01$ . Thus, to very good accuracy, first and second generation left-handed squarks decay through the wino, right-handed squarks decay through the bino.

Given a Higgsino plus Higgs boson lighter than the wino and/or bino, the two-body decays into Higgs bosons discussed in Sec. II become applicable. Since the lighter quarks ( $u, d, c, s$ ) have Yukawa couplings far subdominant to the gauge coupling strengths  $g, g'$ , the cascade in which squarks decay directly into the Higgsinos essentially never occurs. This implies the large QCD-dominated production cross sections of squarks can lead to substantial numbers of Higgs bosons from the cascade decays with only modest mass hierarchy requirements. Moreover, in addition to squark pair production, squark-

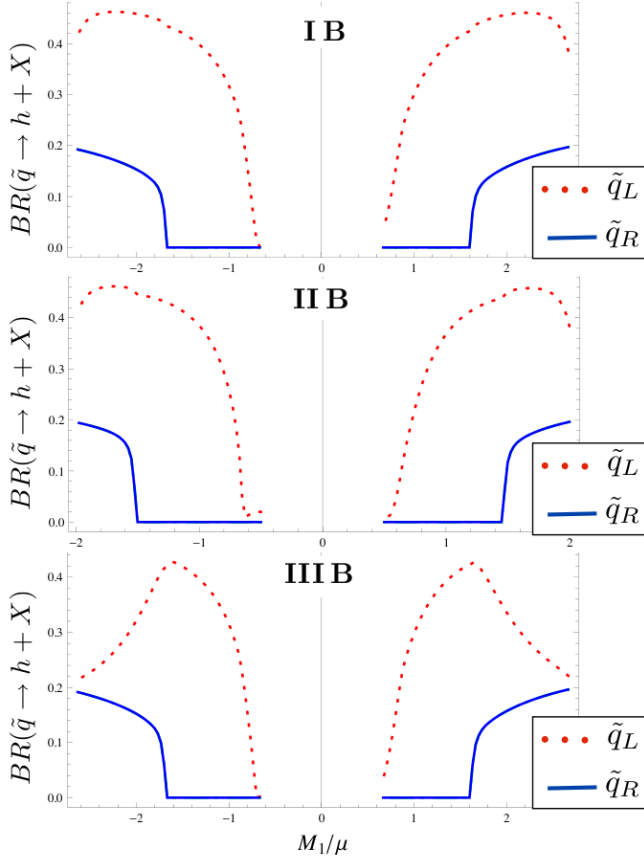


FIG. 2. The branching ratios for decays to the lightest Higgs boson as a function of  $M_1/\mu$ . The MSSM parameters for each plot are the same as the three rows in Fig. 1. Here  $\tilde{q}_L$  refers to the sum of  $\tilde{u}_L$  and  $\tilde{d}_L$  (both components of the electroweak doublet), while  $\tilde{q}_R$  refers to either  $\tilde{u}_R$  or  $\tilde{d}_R$ .

gluino and gluino pair production can also lead to substantial rates of squarks through the two-body  $\tilde{g} \rightarrow \tilde{q}q$ .

We have thus clearly demarcated the superpartner cascades into Higgs bosons as having two largely independent sources, namely

$$\tilde{q}_L \rightarrow q + \tilde{W}; \quad \tilde{W} \rightarrow h/H/A + \tilde{H} \quad (10)$$

$$\tilde{q}_R \rightarrow q + \tilde{B}; \quad \tilde{B} \rightarrow h/H/A + \tilde{H}. \quad (11)$$

This will be useful as we consider variations of gaugino masses and slepton masses.

Gauginos can also decay to sleptons, and it is fairly easy to see what effect they have if they are lighter than the bino and/or wino. For simplicity, consider all three generations of sleptons to be degenerate. If all sleptons are lighter than the bino, we can estimate the branching ratio by just summing over three generations of right-handed and left-handed leptons plus one Higgs doublet. We get

$$BR(\tilde{B} \rightarrow h\tilde{H}^0) \simeq \frac{1}{4} \frac{Y_H^2}{3Y_L^2 + 3Y_e^2 + Y_H^2} \simeq 0.015 \quad (12)$$

(for  $m_{\tilde{L},R} < M_1$ )

where the  $1/4$  comes from for picking just  $h$  from  $(h, z_0, w^+, w^-)$ , assuming  $m_A$  is large. (It is easy to generalize for smaller  $m_A$ .) If left-handed sleptons are lighter than the wino, we get

$$BR(\tilde{W}^0 \rightarrow h\tilde{H}^0) \simeq \frac{1}{4} \frac{Y_H^2}{3Y_L^2 + Y_H^2} \simeq 0.06 \quad (13)$$

(for  $m_{\tilde{L}} < M_2$ ).

So, the effect of all sleptons lighter than the bino is to very efficiently suppress the cascade decay of right-handed squarks to Higgs bosons from about  $1/4$  to about a percent. Conversely, the effect of left-handed sleptons lighter than the wino is to reduce the branching ratio from about  $1/4$  to  $1/16$ . While this suppression is significant, it certainly does not eliminate this decay mode, and illustrates the robustness of finding a Higgs boson within a fairly generic superpartner cascade.

We can study the branching ratios in more detail numerically. As we have already seen, the likelihood of finding a Higgs boson in a complex decay chain originating from a squark can be approximated, to a large extent, by the product:

$$P_{\tilde{q}h} \equiv \text{Br}(\tilde{q} \rightarrow X \rightarrow h + Y) \approx \sum_{\chi_a = \chi_{4,3}^0, \chi_2^\pm} \text{Br}(\tilde{q} \rightarrow \chi_a + \dots) \text{Br}(\chi_a \rightarrow h + \dots), \quad (14)$$

where  $X$  and  $Y$  are other particles or superpartners.

Consider now two interesting regimes for the masses of the Higgs bosons. The first, “large  $m_A$ ”, and the second, “smaller  $m_A$ ”.

### A. Large $m_A$

The first regime we consider is when

$$m_A \gg \min(m_h, |M_2 - \mu|, |M_1 - \mu|), \quad (15)$$

often described as the “decoupling limit”. In this limit, all of the Higgs bosons  $H, A, H^\pm$  are predominantly eigenstates from the second Higgs doublet. These Higgs bosons are much heavier than the lightest Higgs as well as the lighter superpartners in the model. In practice, we take  $m_A \sim 1$  TeV, and thus the scalars  $H, A, H^\pm$  have masses  $\sim 1$  TeV, while  $h$  mixes minimally to  $H$  with ordinary couplings to standard model particles.

#### 1. Higgs in a cascade:

In Fig. 1 we show the branching ratios of  $\chi_{4,3}^0 \rightarrow h + \chi_{1,2}^0, \chi_2^\pm \rightarrow h + \chi_1^\pm$  and in Fig. 2 we show  $P_{\tilde{q}_L h}$  and  $P_{\tilde{q}_R h}$  as a function of  $M_1/\mu$  in the large  $m_A$  regime.

Plot I in Figs. 1, 2 is generated with all the squarks and sleptons set to 1 TeV. Because of using a small value of  $|\mu|$  (namely, 150 GeV), winos are relatively heavier than

the Higgsinos and mix minimally to the rest of the gauginos throughout. As a result, the heavier mass eigenstates ( $\chi_4^0$  and  $\chi_2^\pm$ ) are mostly winos. As indicated in Plot I in Fig. 1, winos decay significantly to the lightest Higgs boson. In fact, for  $M_2 \gtrsim 300$  GeV, wino decay follows the “Goldstone region”: roughly 3/4 of the time the wino decays into longitudinal  $W/Z$  and 1/4 of the time it decays into the lightest Higgs boson. For a large part of the parameter space the mass gaps between  $\chi_3^0$  and  $\chi_{1,2}^0$  are not large enough to allow a two-body decay into the lightest Higgs boson. Once outside the kinematically forbidden zone, however, the branching ratio of the decay  $\chi_3^0 \rightarrow h + \chi_{1,2}^0$  rises quickly with increasing  $M_1$ . In this region,  $M_1/\mu$  is large and  $\chi_3^0$  is mostly a bino.

The same spectrum is used to generate plot I in Fig. 2. Note that the right-handed squarks decay mostly to the bino and so  $P_{\tilde{q}_R h}$  looks almost identical to the branching ratio of  $\chi_3^0$  decaying to Higgs boson. Similarly, the left-handed squarks decay mainly to the winos and  $P_{\tilde{q}_L h}$  follows the partial decay width of  $\chi_4^0$  and  $\chi_2^\pm$  to Higgs bosons. The other feature to note in this plot is that  $P_{\tilde{q}_L h}$  goes down for large  $M_1$ , signifying that the decays of squark to quark plus wino are beginning to be affected by kinematical suppression from the heavy wino.

Plots II in Figs. 1,2 are similar to Plots I except that slightly heavier Higgsinos ( $|\mu| = 200$  GeV) are used. Larger  $M_1/\mu$  is needed in order to open up  $\chi_3^0$  decays to Higgs bosons. A curious rise is seen in  $\chi_4^0$  decays for small  $M_1$ . It is an artifact of decays  $\chi_4^0 \rightarrow W^\pm + \chi_1^\mp$  shutting down, thereby, causing total decay width of  $\chi_4^0$  to shrink. This feature is more prominent for negative  $\mu$ . Even if all parameters in the chargino mass matrices are held fixed, taking  $M_2$  to have the opposite sign of  $\mu$  reduces the splitting among the mass eigenvalues. This results in heavier  $\chi_1^\pm$  and prevents the two-body decay  $\chi_4^0 \rightarrow W^\pm + \chi_1^\mp$  decays even for heavier  $\chi_4^0$ . Once again,  $P_{\tilde{q}_L h}$  and  $P_{\tilde{q}_R h}$  follows the partial decay width of winos and bino respectively. One thing to note is that even though there is a sharp rise in  $\chi_4^0$  and  $\chi_2^\pm$  partial widths for small  $M_1$ , there is no such curious feature in  $P_{\tilde{q}_L h}$ . In this limit,  $M_2 \sim |\mu|$  and decays of squarks to  $\chi_4^0$  and  $\chi_2^\pm$  suffer because of rising Higgsino content in them.

Finally, for Plot III in Figs. 1,2, all parameters are the same as Plots I except that the sleptons are taken be lighter, in this case, 500 GeV. As the wino mass is increased above this value, the wino-like neutralino and charginos begin to decay into slepton modes, reducing the branching fraction to the lightest Higgs boson.

## 2. Boost of a Higgs boson in a Superpartner Cascade

In a typical cascade, a Higgs boson appears from the decay of a massive superpartner. The large release in rest mass results in a large recoil energy, i.e., Higgs bosons from superpartner decays are naturally boosted. This is demonstrated in Fig. 3, which shows that a significant fraction of Higgs bosons are boosted with  $p_T > 200$  GeV

(and even with 300 GeV, as shown). The boost was found by generating samples of 5000 supersymmetric events at different values of  $M_1/\mu$  using PYTHIA v6.4 [32], and plotting the Higgs transverse momenta.

Both of the plots in Fig. 3 are made with  $\mu = 150$  GeV,  $\tan \beta = 10$  and all squarks with mass of 1 TeV. Sleptons have mass of 1 TeV in plot I and 500 GeV in plot II. The presence of light sleptons reduces the fraction of supersymmetric production that leads to a boosted Higgs boson in the cascade. This is due not only does the overall lower fraction of Higgs bosons appearing in the cascades (see plot IIIA and IIIB in Fig. 2) when heavy neutralinos and charginos decay to them, but also fewer of the Higgs bosons in the decay chain are boosted.

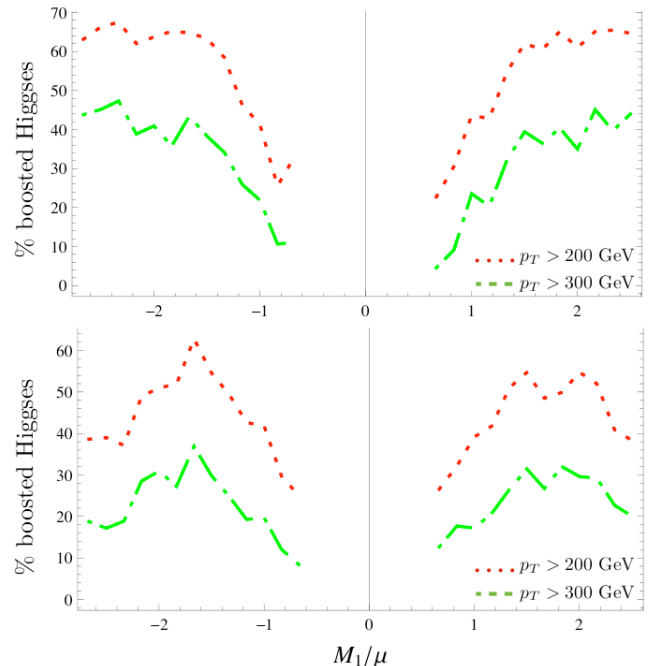


FIG. 3. The fraction (in %) of boosted Higgs bosons as a function of  $M_1/\mu$  with  $M_2 = 2M_1$ ,  $\mu = 150$  GeV and  $\tan \beta = 10$  in samples of events generated by PYTHIA. In the plots the red and dotted lines represent the percentages of Higgs bosons with  $p_T > 200$  GeV and the green dot-dashed lines represent the fraction of Higgs with  $p_T > 300$  GeV. In the left Figure the squark masses are 1 TeV, while in the right Figure the squark masses are 750 GeV. All other relevant soft supersymmetric breaking masses are kept at or above 1 TeV.

## B. Smaller $m_A$

The second interesting regime of the Higgs sector that we consider is smaller  $m_A$ , where

$$m_A < \min(|M_2 - \mu|, |M_1 - \mu|). \quad (16)$$

There are really two distinct regimes of smaller  $m_A$ : the first is when all the Higgs mass eigenstates ( $h, H, A$  and  $H^\pm$ ) are comparable in mass and the CP

even neutral Higgs scalars  $h$  and  $H$  mix maximally among each other. The second is when there is less mixing, but  $H, A, H^\pm$  are light enough to be kinematically accessible to gaugino decay. We will examine both of these cases below.

Interestingly, the branching ratios for  $H \rightarrow b\bar{b}$  and  $A \rightarrow b\bar{b}$  remain the dominant channels decay modes for modest (or larger)  $\tan\beta$  even when decays to gauge boson pairs becomes kinematically accessible. For  $m_A \gg m_Z$ , the mixing angle  $\tan 2\alpha \rightarrow \tan 2\beta$ , and thus  $H$  is mostly  $H_d^0$ . Larger  $\tan\beta$  implies  $\langle H_d^0 \rangle \ll \langle H_u^0 \rangle$ , and thus the 3-point couplings  $HW_\mu W^\mu$ ,  $HZ_\mu Z^\mu$  are suppressed. Analogously, since there is no expectation value for the CP-odd scalar, these 3-point couplings are exactly zero. Thus, the decays into  $b\bar{b}$  remain dominant until  $m_{H,A} \lesssim \min(2\mu, 2M_1, 2M_2)$ , where decays into the lightest gauginos becomes kinematically accessible. This suggests that the  $H, A \rightarrow b\bar{b}$  mode is viable up to well past 200 GeV (twice the smallest allowed Higgsino mass), and for the Study Points in this paper, up to and beyond 300 GeV.

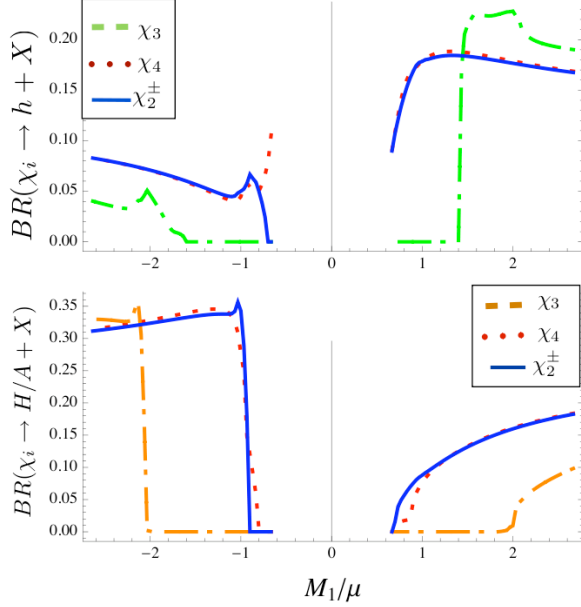


FIG. 4. The branching ratio for decays to a Higgs boson is shown as a function of  $M_1/\mu$  for  $m_A = 150$  GeV,  $|\mu| = 150$  GeV, and  $\tan\beta = 4$ . The upper plot shows the decay rates of heavy gauginos into the lightest Higgs boson, while the lower plot shows the summed decay rates to the heavier Higgs bosons  $H/A$ . The squark and slepton masses are taken to be 1 TeV.

#### IV. MIXED HIGGSINO/BINO AS DARK MATTER

One of the more attractive features of the weak scale supersymmetry with conserved  $R$ -parity is that there ex-

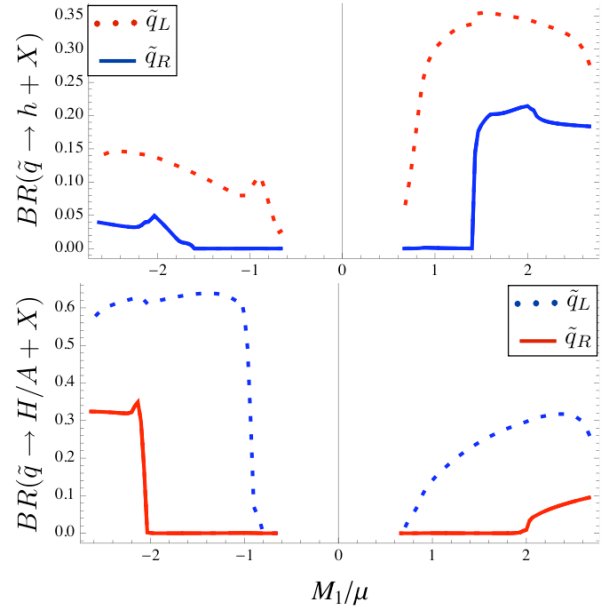


FIG. 5. The branching ratio for squark decays to a Higgs boson as a function of  $M_1/\mu$  for  $m_A = 150$  GeV,  $|\mu| = 150$  GeV, and  $\tan\beta = 4$ . The upper plot shows the decay rate to the lightest Higgs boson, while the lower plot shows the summed decay rate to the heavier Higgs bosons  $H/A$ . As in Figure. 2,  $\tilde{q}_L$  refers to the sum of  $\tilde{u}_L$  and  $\tilde{d}_L$ , while  $\tilde{q}_R$  refers to either  $\tilde{u}_R$  or  $\tilde{d}_R$ . The squark and slepton masses are taken to be 1 TeV.

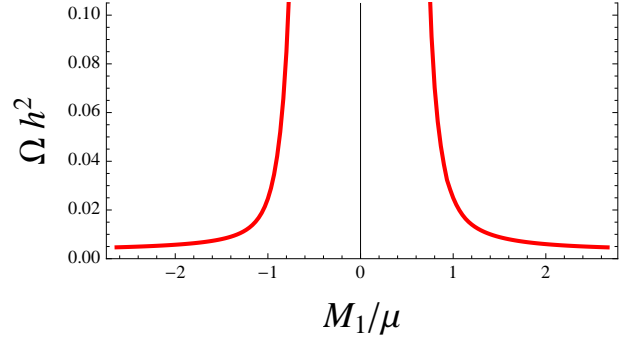


FIG. 6. The LSP relic density as a function of  $M_1/\mu$  with  $M_2 = 2M_1$ ,  $|\mu| = 150$  GeV, and  $\tan\beta = 10$ . The squarks, sleptons, and  $m_A$  were taken to be 1 TeV. The thermal relic density was calculated using micrOMEGAs v2.4 [33].

ists a stable, neutral, colorless, weakly-interacting particle near the electroweak scale. In the post-LEP era, however, the prediction of present dark matter density does not automatically agree with the observation. LEP bounds typically forces the superpartner spectrum to be heavier and hierarchical. In this scenario, neutralinos are closer to pure gauge eigenstates, namely bino, wino and Higgsinos. Avoiding coannihilation and Higgs pole regions, the relic density is generally too large for a bino and too small for Higgsinos and winos. Matching cosmological data seemingly requires rather precise re-



lations among supersymmetry breaking parameters (see e.g. [34]).

Much of these constraints follow from the requirement that the LSP relic density matches the observed cosmological dark matter density. For our purposes, we are content to simply not predict too much dark matter, since other non-thermal sources of dark matter may be present. All of the Study Points considered in the paper automatically have a thermal LSP relic abundance that is at or smaller than the observed cosmological abundance,  $\Omega_{\chi_1^0} h^2 \leq 0.1$ .

In Fig. 6 we show the calculated thermal relic density  $\Omega_{\chi_1^0} h^2$  is plotted as a function of  $M_1/\mu$  for a fixed value of  $|\mu| = 150$  GeV and  $\tan \beta = 10$ . The thermal relic density was calculated using micrOMEGAs v2.4 [33]. All squarks and sleptons were taken to be 1 TeV. This clearly shows the variation of  $\chi_1^0$  relic density as the gaugino/Higgsino content of LSP is changed. For large values of  $M_1/\mu$ , the lightest neutralino is mostly a Higgsino. As is well known, Higgsino-like neutralinos annihilate efficiently into gauge bosons, causing the calculated relic density to be smaller than the cosmological density. As the bino fraction of  $\chi_1^0$  increases with decreasing  $M_1$ , the annihilation rate goes down, and thus relic density goes up. Since the squarks and sleptons are much heavier than the gauginos, the bino rarely annihilates through them. For the specific parameters we considered, we find the annihilation rate can be optimized to give the right relic abundance to match the observed cosmological abundance when  $M_1 \sim |\mu|$ .

Matching the thermal relic density by taking  $M_1 \sim |\mu|$  means bino cannot decay into Higgsinos and Higgs bosons. Given the near independence of  $\tilde{q}_L \rightarrow \tilde{W}$  and  $\tilde{q}_R \rightarrow \tilde{B}$  (c.f. Sec.III), only roughly half of the potential Higgs signal is lost given that right-handed squarks no longer lead to decays into Higgs bosons. We present one Study Points that demonstrates the Higgs signal remains perfectly viable when  $M_1 \sim |\mu|$ .

## V. JET SUBSTRUCTURE ALGORITHM

There are now several interesting techniques that exploit jet substructure to enable better identification of standard model or beyond-the-SM signals [13–16, 23–25, 27, 29, 30, 35–37]. The central idea motivating the elaborate jet manipulation is that it is possible to seek a single “fat jet” (that is, a jet with a particular structure consistent with one coming from a massive particle decay) from the decay products of a boosted particle. Butterworth, Davison, Rubin, and Salam (BDRS) [13] demonstrated that the Higgs boson of the Standard Model could be found with high significance using this technique [13]. Their particular study has been validated by a realistic simulation done by the ATLAS collaboration [20].

The substructure algorithm developed by BDRS [13] to find a Higgs boson has two distinct parts: First deter-

mine whether a jet contains substructure consistent with coming from a Higgs decay to  $b\bar{b}$ . If it passes the criteria, “filter” the jet, improving the resolution of the invariant mass of the candidate resonance jet significantly. In order to identify a jet as a “fat jet”, BDRS stipulate two conditions: the mass of individual subjets are significantly smaller than the mass of the jet (the mass-drop condition) and the splitting of the jet into the two subsets is not too asymmetric. The mass-drop condition basically checks how the jet-mass is distributed in the jet-area, and seeks out a jet that is consistent with one accommodating all the decay products of a massive particle. Given the immense rate for QCD jets, the mass-drop condition alone is not enough. The background jets are, however, dominated by gluon splittings which exhibit soft and collinear singularities. These singularities imply the majority of QCD subjets are asymmetric, so by rejecting particularly asymmetric splittings, the background can be further suppressed.

## Substructure for Supersymmetry

In Ref. [14] we proposed an algorithm to extract a Higgs boson signal using its dominant decay mode,  $h \rightarrow b\bar{b}$  from a new physics event sample. Our algorithm exploits the techniques developed by BDRS, with some additional steps designed to allow our algorithm to be somewhat more efficient than BDRS when applied to busier final states characteristic of new physics. Following the criteria laid out in Sec. III, the simplest superpartner cascade which yields a boosted Higgs is,  $\tilde{q} \rightarrow \chi + j \rightarrow \chi' + h + j$ , which necessarily involves one additional hard parton. More complicated signal events, with multiple extraneous, hard partons are easy to imagine. These hard partons, and their associated showers, can end up in the same fat-jet as the  $h \rightarrow b\bar{b}$ . As these contaminating partons come from heavy particle decay and not from QCD radiation, they can survive the mass-drop and the asymmetry cuts (top and bottom quarks coming from the decay of superpartners are particularly dangerous as they also possess heavy flavor). Consequently, while declustering a fat jet, one may encounter multiple stages (say, “thresholds”) that would pass all substructure criteria cited above.

The BDRS algorithm is designed to consider only the *first* declustering stage that satisfies the mass-drop and asymmetry conditions, and as such, it is more susceptible to false thresholds encountered in new physics events. BDRS jets are built using the inclusive C/A algorithm [39–41], where subjets closer to each other are combined earlier, so the first threshold encountered will be where the subjets are maximally separated. To help distinguish between real and false thresholds, we need to use more information about the subjets. Although the contaminating hard partons are not removed by the mass-drop and asymmetry cuts, they necessarily introduce a new scale into the jet. Rather than select a threshold based

on separation alone, we select the threshold where the subjet kinematics are maximally similar. Specifically, we impose a measure of similarity: maximize subjet hardness weighted by the inter-subjet separation. This measure takes advantage of the isotropic decay scalar particles – the Higgs bosons – that we are interested in. The algorithm [14] is described in full detail below.

### A. Our Algorithm

The first step in our algorithm is to group final state particles, after all showering and hadronization, into “cells” of size  $\Delta\eta \times \Delta\phi = 0.1 \times 0.1$ . All particles in a cell are combined, and the three-momentum of the total is rescaled such that each cell has zero invariant mass [24]. Cells with energy  $< 1$  GeV are discarded, while the rest are clustered into jets. The initial clustering is done using the inclusive C/A algorithm, as implemented in FastJet [42], and taking the jet size to be  $R = 1.2$ . Once the jets are formed, we search for heavy flavor; this is an essential step given that we want to discover the Higgs through its decays to bottom quarks. We  $b$ -tag jets by looking through the event record for  $b$ -mesons or  $b$ -baryons. If there is a  $b$ -flavored object within  $20^\circ$  of a jet direction, we tag the nearby jet as a  $b$ -jet with 60% probability. If there are no  $b$ -flavored objects in the vicinity of the jet in question, the jet is tagged as a  $b$ -jet with a “fake-rate” of 2%. Every  $b$ -tagged jet in the event is then decomposed to search for substructure following the steps below:

1. Undo the last stage of jet-clustering. As a jet is built from a sequence of  $2 \rightarrow 1$  mergings, unclustering one stage yields two subjets. The two subjets  $j_1$  and  $j_2$  are labeled such that  $m_{j_1} > m_{j_2}$ .
2. Following Ref. [13], subjets are checked for the existence of a significant mass drop ( $m_{j_1} < \mu m_j$ ), as well as non-existence of an asymmetry defined by  $y = \frac{\min(p_{Tj_1}^2, p_{Tj_2}^2)}{m_j^2} \Delta R_{j_1, j_2}^2 > y_{\text{cut}}$ . We use  $\mu = 0.68$  and  $y_{\text{cut}} = (0.3)^2$  identical to Ref. [13]. Both subjets are required to be  $b$ -tagged and have  $p_T > 30$  GeV. If these conditions are satisfied, this stage of clustering (say,  $i$ -th) is recorded and then the following is calculated:

$$S_i = \frac{\min(p_{Tj_1}^2, p_{Tj_2}^2)}{(p_{Tj_1} + p_{Tj_2})^2} \Delta R_{j_1, j_2} . \quad (17)$$

The quantity  $S_i$  (namely, similarity) is an indicator of the similarity of the two subjets and is weighted by their separation  $\Delta R_{j_1, j_2}$ .

3. Replace  $j$  by  $j_1$  and repeat from step 1 as long as  $j$  has further subjets.
4. Select the stage of clustering for which  $S_i$  is the largest. We anticipate that the two  $b$ -tagged subjets, at this stage, are most likely to have originated from Higgs decay since they are more likely to be similar to

each other. If the two C/A  $b$ -tagged subjets originate from Higgs decay, the subjets with opening angle  $\Delta R_{j_1, j_2}$  should contain all the perturbative radiation from the  $b\bar{b}$  system by virtue of angular ordering [43]. However, the subjets still tend to include too much contamination from underlying events. We then filter [13] the events: we cluster the jet constituents again using a finer angular scale specific to the jet [we use,  $\min(R_{bb}/2, 0.3)$ ] and retain only the three hardest components ( $b\bar{b}g$ ). Finally, we combine the three subjets and call the resultant a “candidate resonance jet”.

### B. Comparison with BDRS Algorithm

Our algorithm declusters the event entirely, thereby checking multiple thresholds, while the BDRS algorithm only checks a single threshold. In an environment where there are few extraneous partons flying around, such as  $W^\pm H$  production or even supersymmetric Higgs production from short cascades, there are few false thresholds and the two algorithms perform comparably. However, as the number of extra partons (and thus the number of false thresholds) increases, there is a clear difference in efficiency. Any threshold, genuine or not, will stop the BDRS algorithm, while our approach takes in all thresholds and sorts them out using the  $p_T$  similarity. Events with a true threshold masked by a false threshold at larger  $R$  will be missed by BDRS, but captured by our approach. Of course, the similarity variable will not always select out a true threshold from among several, so accuracy is not necessarily increased. Fig. 7, shown below, is a simple demonstration of how our algorithm is more efficient in a crowded environment.

This Figure was generated from a signal sample of 80K PYTHIA-generated events using the spectrum SHSP 3 listed in Table I. The key feature of this spectrum is that the gluino is as light as the squarks, so the signal sample has a significant number squark-gluino associated-production events. The gluinos decay through off-shell squarks, and typically lead to busy, multi-jet events. As a measure of the increased efficiency, we can count the number of event under the putative Higgs peak and compare with the number of events in the bins adjacent to the peaks for each of the algorithms. The significance, defined as  $(\# \text{ events in peak above continuum}) / \sqrt{(\# \text{ continuum events})}$  is larger for the similarity algorithm by a factor of  $\sim 1.2$ . As we will later see, the continuum supersymmetric events are often the largest background to the Higgs peak, so we can expect the complete significance (including SM backgrounds) to increase by roughly the same amount.

It is important to point out that, although we employ this algorithm to find Higgs, all we really check for is a massive particle decaying to 2  $b$  partons. Any heavy multiplet that decays to 2  $b$  should also be selected by our jet algorithm as long as they are boosted. Among



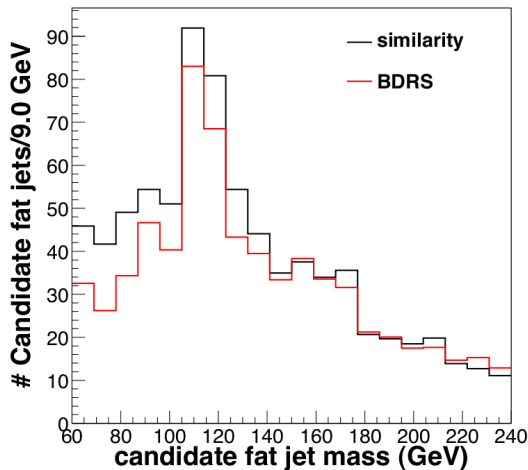


FIG. 7. Comparison of the candidate resonance jet mass using the similarity algorithm (black) and the original BDRS algorithm (red), applied to our  $b$ -tagged fat jet sample. The signal point used for the comparison is SHSP 3 (see Table I), and the vertical axis has been rescaled to correspond to an integrated luminosity of  $\mathcal{L} = 10 \text{ fb}^{-1}$ . While the accuracy of the two algorithms is similar, the similarity algorithm is more efficient.

SM particles we expect to find  $Z \rightarrow b\bar{b}$ <sup>2</sup>. Also, when both  $H$  and  $A$  are light and decay to  $b\bar{b}$ , our algorithm can discover Higgs bosons as long as they are produced in a superpartner cascade.

## VI. RESULTS

Having demonstrated sparticle cascade decays as a viable, important source of boosted Higgs bosons and described our substructure algorithm in detail, we now demonstrate the effectiveness of our proposal. To best convey our results, we first propose a collection of Study Points on which we use the candidate resonance jet finding algorithm. While by no means exhaustive, the Study Points have a diverse set of MSSM parameters. After introducing the Study Points, we then list the set of backgrounds we considered for this work and show the way in which sets of conventional cuts can be used to reduce these. The candidate resonance jet finding algorithm is then run on this set of rarefied events (both signal and background events). Finally, masses of the candidate resonance jets are plotted to estimate the signal significance.

<sup>2</sup> In practice, as light jets can occasionally fake  $b$ -jets, any boosted, heavy particle which decays hadronically ( $t, W, \dots$ ) has a chance of being picked up by the substructure algorithm.

### A. Supersymmetric Higgs Study Points

The efficiency of our algorithm to find Higgs bosons is demonstrated on a set of benchmark points, Supersymmetric Higgs Study Points (SHSPs), tabulated in Table I. These Study Points are grouped into three categories.

- Study Points 1,2 represent spectra in the decoupling limit ( $m_A = 1 \text{ TeV}$ ). In SHSP 1a and 1b the LSP is mostly bino, all squarks are at 1 TeV, and the sleptons are at 1 TeV and 350 GeV respectively. In SHSP 2a and 2b the LSP is a maximal mixture of Higgsinos and bino. In SHSP 2a once again we use heavier squarks and sleptons while slightly lighter squarks and sleptons are used in SHSP 2b.
- SHSP 3 has  $M_1 \simeq |\mu|$  and large  $m_A$ , such that the LSP has a thermal relic density that matches cosmological measurements.
- The final set of Study Points, SHSP 4,5 ( $|\mu| = 150 \text{ GeV}$ ) and SHSP 6 ( $|\mu| = 200 \text{ GeV}$ ) are representatives of spectra in the smaller  $m_A$  region. The main difference between SHSP 4,6 versus SHSP 5 is the sign of the  $\mu$  term. As shown in Fig. 5, when  $m_A$  is low the sign of  $\mu$  greatly influences which Higgs bosons the gauginos decay into. For SHSP 4,6, decays to  $h$  predominate, while  $H/A$  predominate in SHSP 5.

To simulate the supersymmetric signal, we use PYTHIA v6.4 to generate parton level events, with subsequent showering and hadronization. The lowest-order, inclusive superpartner production cross sections are large ( $\mathcal{O}(\text{pb})$ ) and are listed for all Study Points in Table I. These cross sections are somewhat misleading, since the quoted cross sections also include electroweak production of light charginos and neutralinos. In the scenarios we are considering, the lightest charginos and neutralinos have a large Higgsino component and thus large couplings to the  $Z$  boson. As a result, the LHC cross sections for neutralino pair production  $\chi_1^0 \chi_2^0$ , chargino pair production  $\chi_1^\pm \chi_1^\mp$  and associated chargino-neutralino production  $\chi_{1,2}^0 \chi_1^\pm$  are all quite large,  $\mathcal{O}(0.5 - 1 \text{ pb})$ . While a large chargino/neutralino production cross section will likely enable the discovery of new physics, light neutralinos and charginos do not decay to Higgs bosons so these events are of no use for a Higgs search. Therefore, in order to fairly judge our Higgs-finding algorithm, we have included the fraction of supersymmetric events containing a Higgs boson ( $h/H/A$ ) in Table I. This fraction was calculated by counting the number of on-shell Higgs bosons, without any kinematic cuts, in samples of PYTHIA-generated supersymmetric events. The final row in Table I,  $\sigma_{h/H/A}$ , is simply the inclusive supersymmetric cross section times the fraction of supersymmetric events containing a Higgs boson.

	SHSP 1a / SHSP 1b	SHSP 2a / SHSP 2b	SHSP 3	SHSP 4	SHSP 5	SHSP 6
$\tan\beta$	10	10	10	5	6.5	10
$M_1$	300 GeV	150 GeV	163 GeV	200 GeV	200 GeV	300 GeV
$M_2$	600 GeV	300 GeV	400 GeV	400 GeV	400 GeV	600 GeV
$M_3$	2.1 TeV	1.05 TeV	1.0 TeV	1.4 TeV	1.4 TeV	2.1 TeV
$\mu$	150 GeV	150 GeV	200 GeV	200 GeV	-150 GeV	150 GeV
$m_A$	1 TeV	1 TeV	1 TeV	150 GeV	150 GeV	200 GeV
$a_t$	900 GeV	-900 GeV	900 GeV	2.04 TeV <sup>a</sup>	1.4 TeV	900 GeV
$m_{\tilde{q}}$	1 TeV	1 TeV/750 GeV	1 TeV	1 TeV	1 TeV	1 TeV
$m_{\tilde{l}}$	1 TeV/350 GeV	1 TeV/350 GeV	350 GeV	1 TeV	1 TeV	1 TeV
$m_h$	116 GeV	117 GeV	116 GeV	114 GeV	115 GeV	115 GeV
$m_H$	1 TeV	1 TeV	1 TeV	161 GeV	157 GeV	202 GeV
$m_A$	1 TeV	1 TeV	1 TeV	150 GeV	150 GeV	200 GeV
$m_{H^\pm}$	1 TeV	1 TeV	1 TeV	169 GeV	170 GeV	216 GeV
$\chi_1$	138 GeV	110 GeV	140 GeV	157 GeV	136 GeV	138 GeV
$\chi_2$	-158 GeV	-161 GeV	209 GeV	-207 GeV	-163 GeV	-158 GeV
$\chi_3$	206 GeV	174 GeV	-209 GeV	227 GeV	210 GeV	306 GeV
$\chi_4$	625 GeV	338 GeV	429 GeV	433 GeV	426 GeV	623 GeV
$\chi_1^+$	148 GeV	137 GeV	191 GeV	187 GeV	152 GeV	148 GeV
$\chi_2^+$	625 GeV	337 GeV	429 GeV	433 GeV	426 GeV	623 GeV
$\sigma_{\text{tot}}$	3.9 pb	5.8 pb / 8.07 pb	2.76 pb	2.4 pb	4.1 pb	4.0 pb
% Higgs	4.5%/3.4%	4.2%/6.8%	6.6%	12.8%	8.6%	7.0%
$\sigma_{h/H/A}$	0.18 pb/0.13 pb	0.24 pb/0.55 pb	0.18 pb	0.31 pb	0.35 pb	0.28 pb

<sup>a</sup>  $a_b = a_t$  for this point as well

TABLE I. The parameters, part of the spectrum, and some relevant collider information for the Study Points used in this analysis. The spectrum was computed with SUSPECT2 [44]. The quoted cross section is determined at lowest order for the LHC operating at a center of mass energy of  $\sqrt{s} = 14$  TeV. See the text for the definition of % Higgs and  $\sigma_{h/H/A}$ .

### Backgrounds and Cuts:

The primary SM backgrounds we consider are:

- $\bar{t}t$ +jets
- $W/Z$ + heavy flavor
- $W/Z$ + jets
- $\bar{t}t + \bar{b}b$

These backgrounds are familiar from many supersymmetry/BSM searches. They have large cross sections, multiple jets, some of which are  $b$ -jets, and sources of missing energy from vector boson decays. The background events are first generated at parton-level using ALPGEN v13 [45] and are then showered and hadronized using PYTHIA v6.4<sup>3</sup>. We also use the ATLAS tune [46] in PYTHIA to model the underlying event. Jet manipulation is done using FastJet [42]. We do not perform any detector simulation or smearing of jets. A realistic ATLAS/CMS specific search in the spirit of Ref. [20] is beyond the scope of this work. However, since high  $p_t$  jets result in a large amount of energy deposited in the calorimeter cells where energy resolution is excellent, we

do not expect smearing to significantly modify our results.

Before we run our substructure algorithm, we introduce cuts to isolate the signal from the background. Rather than tailoring the cuts to each specific SHSP point, we choose a more generic set which can be applied to all Study Points. In particular, we use:

1.  $\cancel{E}_T > 300$  GeV.
2.  $3^+$  jets, at least one of which is tagged as a  $b$ -jet. To be counted as a jet, we require  $p_T > 200$  GeV – the  $p_T$  requirement on the jets is set so high because we want to capture an entire boosted object (ideally a Higgs) within a single jet. As explained in Sec. V, objects will be reconstructed from sub-jets contained within individual high- $p_T$  jets rather than combining multiple jets. We impose a pseudorapidity cutoff of  $|\eta| < 4.0$  for jets which are not flavor-tagged, while  $b$ -tagged jets are restricted by the pseudorapidity extent of the tracker,  $|\eta| < 2.5$ .
3. No isolated leptons with  $p_T > 20, |\eta_\ell| < 2.5$ .
4.  $H_T^{\text{jets}} = \sum_i p_{T,i} > 1.0$  TeV, where the sum extends over all jets indexed by  $i$ .

<sup>3</sup> All events generated with ALPGEN using CTEQ5L parton distribution functions and default options for factorization/renormalization scheme.

Large missing energy, large  $H_T^{\text{jets}}$ , and high jet multiplicity are often the characteristics of new physics and, in particular, of weak scale supersymmetry with  $R$ -

parity<sup>4</sup>. These variables are widely used in supersymmetric searches and we use them here. After  $\cancel{E}_T$  and  $H_T^{\text{jets}}$  cuts, the biggest background is by far  $t\bar{t}$ +jets. In order to suppress the  $t\bar{t}$ +jets further we introduce a lepton veto; the logic behind this cut is that any  $t\bar{t}$ +jets events which pass the large  $\cancel{E}_T$  cut most likely contain at least one leptonic  $W^\pm$ .

We collect all events that pass our preliminary cuts and run the substructure algorithm described in Sec. V. Events which pass the substructure selection have at least one  $b$ -jet with substructure and, consequently, at least one candidate resonance jet.

The assumed background cross sections and their efficiencies under the imposed cuts are summarized below in Table II. To show how substructure cuts affect the signal and background, we have broken up the efficiencies into two stages. The first stage,  $\epsilon_{\text{cuts}}$ , is calculated after the ‘conventional’ cuts –  $\cancel{E}_T$ ,  $H_T^{\text{jets}}$ , jet multiplicity and lepton veto – have been imposed. Then, after running the substructure algorithm, the surviving events are counted to determine  $\epsilon_{\text{cuts}+\text{subs}}$ .

Process	$\sigma$	$\epsilon_{\text{cuts}}$	$\epsilon_{\text{cuts}+\text{subs}}$
$t\bar{t} + 0 \text{ jet}$	474 pb	0	0
$t\bar{t} + 1 \text{ jet}$	248 pb	$9.2 \times 10^{-6}$	$1.62 \times 10^{-6}$
$t\bar{t} + 2^+ \text{ jet}$	132 pb	$2.1 \times 10^{-4}$	$4.84 \times 10^{-5}$
$t\bar{t} + b\bar{b}$	0.83 pb	$1.9 \times 10^{-4}$	$4.6 \times 10^{-5}$
$W(\ell\nu) + 2 \text{ jets}$	127 pb	$2.3 \times 10^{-6}$	0
$W(\ell\nu) + 3^+ \text{ jets}$	50 pb	$2.3 \times 10^{-4}$	$1.08 \times 10^{-5}$
$Z(\bar{\nu}\nu) + 2 \text{ jets}$	80 pb	0	0
$Z(\bar{\nu}\nu) + 3^+ \text{ jets}$	29 pb	$2.3 \times 10^{-4}$	$1.47 \times 10^{-5}$
$Z(\bar{\nu}\nu) + b\bar{b}$	1.4 pb	0	0
$Z(\bar{\nu}\nu) + b\bar{b} + \text{jet}$	1.4 pb	$3.5 \times 10^{-4}$	$6.94 \times 10^{-5}$
$W(\ell\nu) + b\bar{b}$	1.1 pb	$2.6 \times 10^{-6}$	0
$W(\ell\nu) + b\bar{b} + \text{jet}$	2.2 pb	$1.1 \times 10^{-4}$	$3.6 \times 10^{-5}$
SHSP 1A	3.92 pb	0.015	$3.7 \times 10^{-3}$

TABLE II. Signal 1A and background cross sections and efficiencies. The efficiency for the other Study Points is similar. All backgrounds were generated with parton level cuts on jets:  $p_{T,j} > 30$  GeV (25 GeV for  $t\bar{t}$  + jets),  $|\eta_j| < 4.0$ ,  $\Delta R_{jj} > 0.4$ . An additional cut  $\cancel{E}_T > 75$  GeV was used for all  $W/Z$  backgrounds, while  $|\eta_b| < 2.75$  was added for all heavy-flavor events. All background cross sections are LO except for  $t\bar{t}$  + jets, which has been rescaled to the NLO MCFM [47] result  $\sigma = 855$  pb ( $K \sim 1.8$ ).

As can be seen from the Table, the conventional cuts are quite effective at reducing the background. The signal efficiency under the conventional cuts looks low. However, as explained in Sec. VI A, many supersymmetric events for these Study Points come from electroweak

chargino/neutralino pair production which do not contain the sufficient energy or jet multiplicity to pass our cuts; the efficiency for squark/gluino initiated events is higher. Requiring jet substructure suppresses the background further relative to the signal, however the real power from substructure comes in the shape of the jet-mass distribution. Therefore, the final step in our search strategy is to plot the invariant mass of all candidate resonance jets and look for a peak consistent with a Higgs boson. The candidate resonance jet mass plots for each of the 8 benchmark Study Points in Table I are presented in the following sub-sections. To break up the results, we have grouped the Study Points into the same three categories used in Table I: high- $m_A$ , low- $m_A$ , and one Study Point with a LSP thermal relic density that matches cosmological observations.

In all of the following plots, the contribution from *all* supersymmetric events (inclusive superpartner production) are shown together on top of the SM background. While the supersymmetric contribution contains our signal, Higgs bosons from sparticle decays, it also contains new backgrounds. Top quarks and  $W/Z$  bosons will also be copiously produced in cascade decays and can occasionally pass the substructure cuts. In fact, in several circumstances this supersymmetric background is larger than the SM backgrounds.

## B. High- $m_A$ points: SHSP 1a/1b, 2a/2b

The first of the high- $m_A$  points, SHSP 1a and 1b, are characterized by small  $\mu$ . The large  $m_A$  kinematically forbids squark decays to other Higgs states ( $H/A/H^\pm$ ), while the low  $\mu = 0.5M_1 = 150$  GeV implies a very Higgsino-like LSP and thus large branching fractions  $\chi_2^\pm \rightarrow h + \chi_1^\pm$ ,  $\chi_{3,4} \rightarrow h + \chi_{1,2}$ . These points are ideally suited to our analysis, and the resulting candidate resonance jet mass plot, Fig. 8 verifies this. The peak arising from Higgs decay is unmistakable over the relatively featureless SM background.

The small shoulder to the left of the Higgs peak comes from  $Z \rightarrow b\bar{b}$  events. Higgs bosons and the  $Z$  are produced in relatively equal amounts for these two points, due to the arguments presented in Sec. II. However, the  $Z \rightarrow b\bar{b}$  branching fraction is only 1/6 as large as  $h \rightarrow b\bar{b}$ , and the resulting  $Z$  peak is small.

The only difference between SHSP 1a and 1b is the mass of the sleptons. In SHSP 1b, the sleptons are light enough that the heavier charginos and neutralinos can decay into them. As demonstrated in Figs. 1,2, new chargino/neutralino decay modes imply a smaller fraction of decays to Higgs bosons, and thus a smaller signal. However, comparing the top and bottom plots in Fig. 8, we can see that the rate decrease to due decays to sleptons of mass  $M_1 < m_{\tilde{l}} < M_2$  is quite minor.

To get a quantitative idea of how well our algorithm can find the Higgs, we estimate the significance of the

<sup>4</sup> Due to our large jet- $p_T$  requirement,  $H_T^{\text{jets}}$  calculated with our definition can be quite different than the sum of all visible transverse energy in the calorimeters (often referred to as  $H_{T,\text{cal}}$ ). However,  $H_{T,\text{cal}}$ , which we would rely on for triggering, will always be bigger than  $H_T^{\text{jets}}$ .

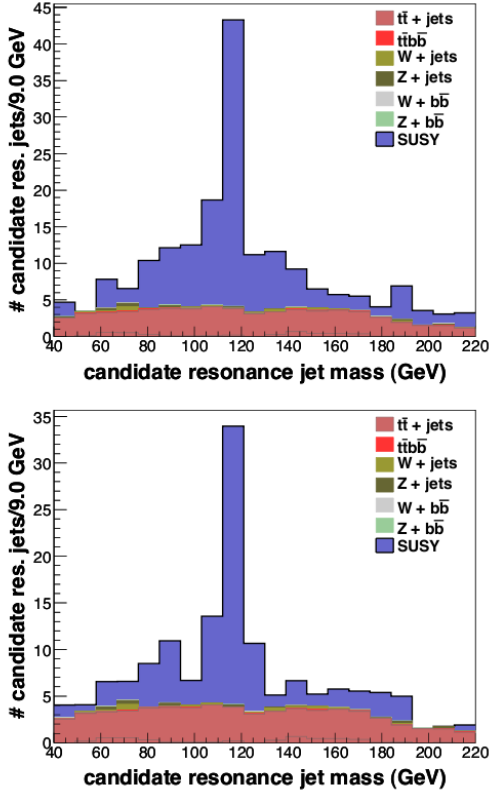


FIG. 8. Distribution of the candidate resonance jet mass normalized to  $10 \text{ fb}^{-1}$  of integrated luminosity at 14 TeV center of mass energy. The contribution from supersymmetric particles is shown in blue for points SHSP 1a (top) and SHSP 1b (bottom). Standard Model contributions, which come primarily from  $t\bar{t} + \text{jets}$ , are indicated by the red and green histograms.

Higgs peak on top of the SM and continuum new physics background. We determine the SM plus continuum contribution using the same simple method as in Ref. [14]; the histograms 1 – 2 bins on either side of the Higgs peak are connected with a line, and anything within the resulting trapezoid is counted as background. To check the veracity of this procedure, we have looked back into the signal events and assigned each event with a candidate resonance jet to an initial parent parton ( $t/W/Z/h$ ) according to which heavy particle is closest in  $\Delta R$ . We find the fat-jets with a parent Higgs are indeed confined to the peak and neighboring bins. Events with a  $Z$  parent are similarly confined to the bins near  $m_Z$ , while the continuum events are composed of  $t/W$  events. Using the peak  $-1/+0$  bins to define the signal region (meaning the bins  $-2/+1$  on either side of the peak are used to determine the background), we find  $\mathcal{S} = S/\sqrt{B} \cong 7.9$  for point SHSP 1a. The same procedure, taking the signal region to be the peak  $\pm 1$  bins, gives  $\mathcal{S} = 9.6$  for point SHSP 1b. These significances are just rough estimates. We have taken quite aggressive conventional cuts to render the SM background as small and featureless as possible; less strict cuts may lead to higher significances,

as would optimization of the cuts for each SHSP point.

The next two high- $m_A$  points are more challenging for three reasons. First, points 2a and 2b have a smaller  $M_1$ . As we saw in Figs. 1,2, a lower  $M_1/\mu$  means fewer Higgs bosons are produced from squark cascades. Second, lowering  $M_1$  while holding  $M_1 : M_2 : M_3$  ratio fixed implies a much lighter gluino. While the gluinos are light in this scenario, they are still capable of decaying to on-shell squarks, so supersymmetric events originating from gluinos – either from gluino pair production or squark-gluino associated production – have more jets than events originating from squark pairs. Additionally, because gluinos decay democratically to all species of squarks, gluino cascades can easily include top and bottom quarks. The third difficulty with 2a and 2b comes from right-handed squarks. Right-handed squarks, produced either in pairs or associated with a left-handed squark or gluino, decay to bino plus jet, with the bino in this spectra spread between  $\chi_1, \chi_2$ , and  $\chi_3$ . However, as can be seen from Table. II, the mass-gaps among the three lightest neutralinos are small enough so that most two-body decay modes are kinematically forbidden; the neutralinos decay instead via an off-shell  $W/Z/h$  plus a lighter chargino/neutralino. Off-shell, hadronic decays quickly lead to an increase in the number of hard partons in the event. For example, a typical signal process involving one right-handed squark:  $pp \rightarrow \tilde{q}_L \tilde{q}_R$  followed by  $\tilde{q}_L \rightarrow \chi_4^0 + j \rightarrow \chi_1^0 + h + j$  and  $\tilde{q}_R \rightarrow \chi_3^0 + j \rightarrow \chi_1^0 + 3j$  involves 4 extra hard partons, any one of which can fall in the same fat-jet as the Higgs boson. Longer cascades, coming from gluino production or more decay steps, are easy to imagine and will contain even more hard partons.

When extra partons from superpartner decays are erroneously combined with all or part of a Higgs candidate, the jet mass becomes smeared. The smearing is exacerbated by the fact that, following BDRS, we take the three hardest subjets during filtering to define the candidate resonance jet. Such a procedure remarkably improves the mass resolution of a Higgs jet when the correct threshold is identified and none of the extra hard partons produced in association with the Higgs is inside the Higgs cone. The three hard partons during filtering then correctly capture  $b\bar{b}$  from Higgs as well as the first radiation inside the  $b\bar{b}$  system. On the other hand, if there is an extra hard parton inside the  $b\bar{b}$  system, the filtered resonance jet may end up containing  $b\bar{b} + \text{hard parton}$  instead of being  $b\bar{b} + \text{radiation}$  and consequently having a skewed invariant mass. This smearing is clearly visible in Fig. 9 and creates the feature extending from the Higgs peak to higher mass. However, despite all the contamination from auxiliary hard partons, the Higgs peak is still quite visible. Perhaps more elaborate subjet algorithms could be used to clean up the high-mass tail further.

Moving from 2a to 2b, the squark mass decreases. Lighter squarks are produced even more prodigiously, as reflected in the enormous superpartner cross section, however they impart a smaller boost on their decay products. The increased production of right-handed squarks

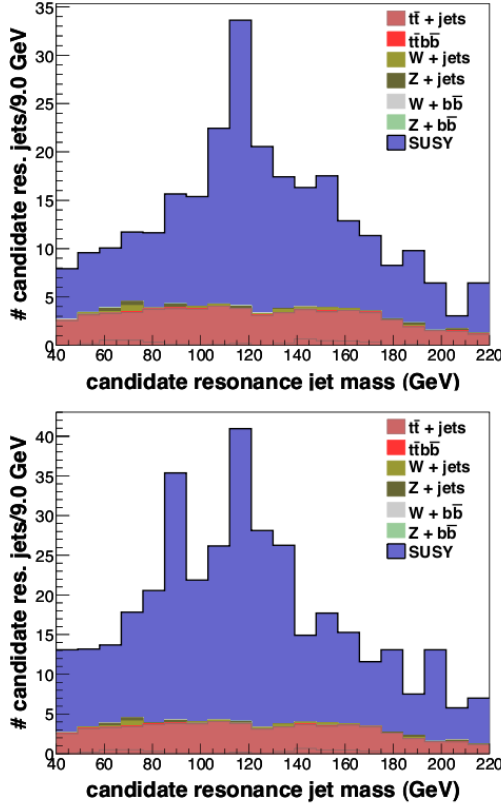


FIG. 9. Distribution of the candidate resonance jet mass in points SHSP 2a (top) and SHSP 2b (bottom). As in Fig. 8 we assume  $10 \text{ fb}^{-1}$  of integrated luminosity and a 14 TeV center of mass energy.

in SHSP 2b, a factor of  $\sim 4$  compared to point 2a is responsible for the increased number of supersymmetric events away from the Higgs peak. The slepton mass in 2b is also smaller than in 2a, however this has only a small effect since the sleptons are still too heavy for the higher-tier charginos and neutralinos to decay into,  $m_{\tilde{l}} > M_2$ . Estimating significance in the same way as we did for SHSP 1a/b and using  $-1/+2$  bins to define the signal region, we find a significance of (3.8, 5.6) for points SHSP (2a, 2b).

Having seen the effects of decreasing the squark mass, it is natural to ask what happens if we do the opposite and raise  $m_{\tilde{q}}$  and  $M_3$  while keeping the rest of the supersymmetry parameters fixed. The squark/gluino mass sets the scale for the boost of its subsequent decay products, including any Higgs bosons. One may worry that a higher sparticle scale would lead to Higgs decay products which are so boosted that finite detector granularity or the need to b-tag multiple subjects would render our algorithm useless. This does not occur, however, as is evident in the distribution of the subjet angular scale  $R_{bb}$ . We find a rather flat distribution between  $0.3 < R_{bb} < 1.2$ , which persists even as  $m_{\tilde{q}}/M_3$  is raised to several TeV (squark with mass beyond 3 TeV have such low production cross

section that they become phenomenologically irrelevant at the LHC). Therefore, even if granularity/tagging inefficiencies ruin the most highly boosted Higgs bosons, the broad tail of  $R_{bb}$  indicates that our algorithm can remain viable throughout the range of interesting squark masses.

### C. Relic Point: SHSP 3

The parameters of point SHSP 3 have been chosen such that the LSP has a thermal relic abundance that matches cosmological observations for the dark matter density. As described in Sec. IV, this requires delicately adjusting  $M_1 \simeq |\mu|$  to get the right bino/Higgsino admixture in the LSP. Point SHSP 3 also has light sleptons, however the branching fraction to Higgs bosons is still high enough for our analysis to be successful. The cascade of superpartner decays contain more  $Z$  than  $h$ , due to the smaller value of  $M_1$ , but the Higgs peak remains clearly visible.

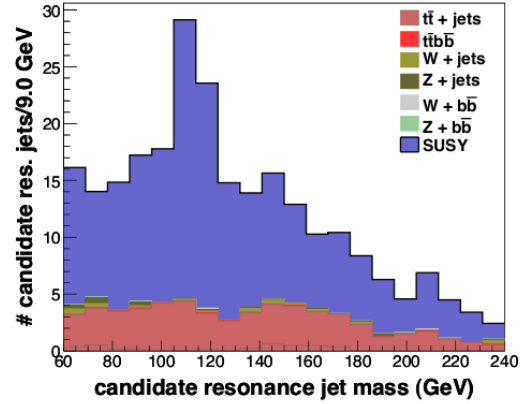


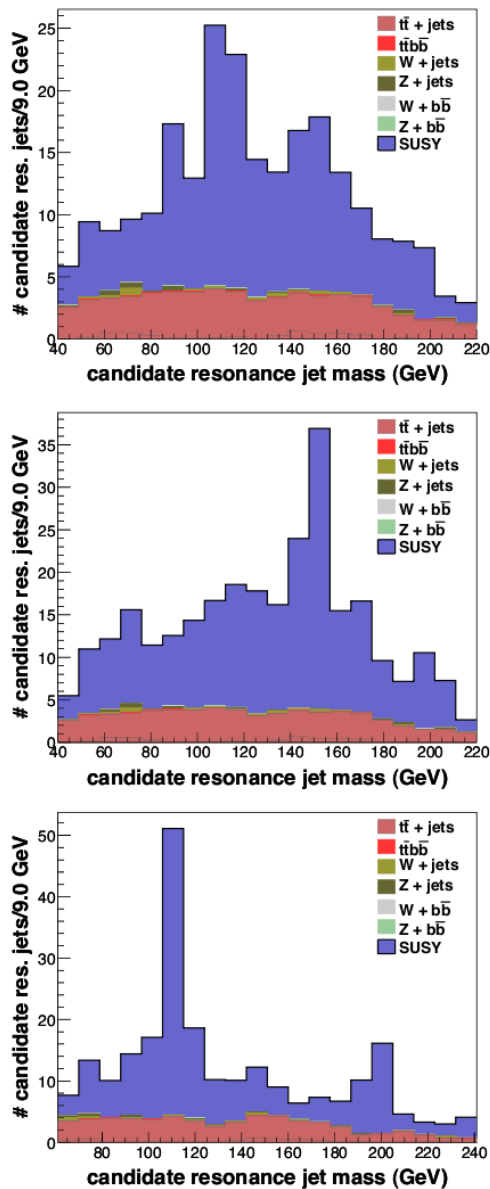
FIG. 10. Distribution of the candidate resonance jet mass in point SHSP 3. The parameters for this point were chosen to produce the correct dark matter relic abundance for the LSP. As in Fig. 8 we assume  $10 \text{ fb}^{-1}$  of integrated luminosity and a 14 TeV center of mass energy.

### D. Low- $m_A$ points: SHSP 4-6

The final set of Study Points have smaller  $m_A$  and a small value for  $\tan \beta$ . The region of smaller  $m_A$ , small  $\tan \beta$  is known to be difficult for traditional MSSM Higgs boson searches, so these points serve as an important test of our algorithm. To ensure the lightest Higgs boson has a mass that exceeds the LEP bound, we allow larger mixing in the stop (and sbottom) sectors. These Study Points are therefore quite similar to the “maximal-mixing” scenario often considered in collider searches [48].

Perhaps the most interesting consequence of  $m_A \ll m_{\tilde{q}}, M_2$ , is that the heavier Higgs bosons  $H/A$  also appear in the superpartner decay cascades. For  $m_H, m_A \simeq$

150 GeV, the  $H/A$  decay predominantly into  $b\bar{b}$  and are light enough that they will emerge from sparticle decays carrying a substantial boost. With these characteristics,  $H/A$  will be captured by our algorithm. This opens the exciting possibility, shown in fig. (VID), of discovering multiple distinct Higgs bosons with a single analysis.



Distribution of the candidate resonance jet mass in points SHSP 4 (top), SHSP 5 (middle), SHSP 6 (bottom). As in Fig. (8) we assume  $10 \text{ fb}^{-1}$  of integrated luminosity and a 14 TeV center of mass energy.

In SHSP 4, the top plot of Fig. VID, heavier charginos and neutralinos decay to  $h$  rather than  $H/A$  making the  $h$  peak unmistakable. Some  $H/A$  are present, and lead to the feature near  $m_A = 150$  GeV. Given the size of the  $m_A$  feature and its proximity to the top mass, detector resolution effects, which we have treated very simply in this paper, become more important and need to be taken

into account correctly.  $H/A$  discovery will likely require a more specialized analysis, but it is certainly possible that both  $H/A$  and  $h$  could be discovered with this technique given sufficient integrated luminosity.

In point SHSP 5, the  $\mu$  term is negative. With  $\mu$  and  $m_A$  similar in magnitude, the Higgs mixing matrix becomes particularly sensitive to the relative sign between these two mass parameters and cancellations can occur once couplings are expressed in terms of mass eigenstates. For  $\mu < 0$ , the  $h$  coupling to higher-tier charginos/neutralinos is suppressed by one such cancellation, and cascade decays to  $H/A$  are more likely. We can clearly see this effect in fig. (VID); the  $h$  peak is barely visible over the continuum new physics events, while the narrow  $H/A$  peak at 150 GeV is clearly evident.

The final point, SHSP 6, has exactly the same supersymmetry parameters as SHSP 1a except  $m_A = 200$  GeV. This is the ideal point for detecting both the light and heavy Higgs bosons with a single analysis. The  $m_A$  is low enough that  $\chi_4$  and  $\chi_2^\pm$  have a moderate branching ratio to  $H/A$ , while  $m_A$  is heavy enough to avoid getting mistaken for new physics continuum or a top quark. Taking the signal region to be  $-0/+1$  bins ( $-1/+1$ ) around the  $h$  peak, we find a significance of (3.9, 8.2) for points (SHSP 4, SHSP 6). Repeating the same procedure around the  $H/A$  peak, we find a significance of (5.2, 4.5) for (SHSP 5, SHSP 6) using signal regions  $-1/+0$  bin.

Low values for  $m_A$  imply light charged Higgs bosons, which are constrained by the flavor process  $b \rightarrow s + \gamma$ . While the specific spectra we are looking at have  $b \rightarrow s + \gamma$  slightly larger than the experimentally allowed range [44, 49], slight changes in the spectrum, such as lowering the third generation squark masses or introducing squark mixing can introduce cancellations and significantly alter the branching ratio  $b \rightarrow s + \gamma$  [50]. These changes to the spectrum need not effect the supersymmetric Higgs signal. Therefore, in the same spirit as [3, 4], we focus on direct Higgs detection prospects and ignore indirect constraints for the time being.

## VII. DISCUSSION

The power of using jet substructure with boosted Higgs decays into  $b\bar{b}$  suggests the search for the MSSM Higgs bosons should be entirely rethought and redone, with full detector simulations. Our estimates, without jet energy smearing and without a realistic detector simulation, suggest that with less than  $10 \text{ fb}^{-1}$  of data at  $\sqrt{s} = 14$  TeV, signal significance can exceed 5 for the  $h \rightarrow b\bar{b}$  channel alone given total superpartner production rate of order a few pb. This is possible given the outstanding mass resolution of our reconstruction technique combined with the power that jet substructure provides in discriminating Standard Model and supersymmetric backgrounds. We have been relatively conservative in our candidate resonance jet finding algorithm given our flat  $b$ -tagging



efficiency: we required a triple  $b$ -tag – the original jet as well as two subjects. Nevertheless, our estimates of signal significance are just that – estimates. We urge the ATLAS and CMS collaborations to carry out full detector simulations, along the lines of what was done by ATLAS to study the boosted Higgs into  $b\bar{b}$  mode in the Standard Model [20].

The notion that both  $h$  as well as  $H$  and  $A$  could be found using jet substructure techniques is particularly interesting given the difficulty that conventional search strategies have within the smaller  $m_A$  and smaller  $\tan\beta$  region. The ATLAS and CMS TDR suggest fully covering the MSSM parameter space requires considerable integrated luminosity, 60-100  $\text{fb}^{-1}$ . Our technique has the potential to cover this region much more rapidly.

It is interesting that the MSSM parameter region most favorable to finding a signal of Higgs bosons is also the one with the least fine-tuning, namely, small  $\mu$  (e.g. [51]). Nevertheless, gaugino mass unification, and other aspects of the superpartner hierarchy are somewhat less constrained.

Finally, finding evidence for Higgs bosons within a new physics event sample provides an incredibly important

connection between the new physics and the Higgs sector – i.e., the Higgs sector is necessarily coupled with the new physics. This connection can be established far faster than sorting out which kind of new physics is present based on the population of different BSM search channels. The generic search strategy proposed here builds on our previous paper [14], demonstrating the power of this method applied to the MSSM with a neutralino, or neutralino-equivalent, lightest supersymmetric particle.

## ACKNOWLEDGMENTS

GDK thanks Fermilab and the Perimeter Institute and TSR thanks Weizmann Institute and Fermilab for hospitality where part of this work was completed. This work was supported in part by the US Department of Energy under contract number DE-FG02-96ER40969 (GDK, TSR, MS). AM is supported by Fermilab operated by Fermi Research Alliance, LLC under contract number DE-AC02-07CH11359 with the US Department of Energy.

- 
- [1] M. S. Carena, H. E. Haber, S. Heinemeyer, W. Hollik, C. E. M. Wagner and G. Weiglein, Nucl. Phys. B **580**, 29 (2000) [arXiv:hep-ph/0001002].
  - [2] J. F. Gunion, P. Kalyniak, M. Soldate and P. Galison, Phys. Rev. D **34**, 101 (1986); A. Stange, W. J. Marciano and S. Willenbrock, Phys. Rev. D **49**, 1354 (1994); J. F. Gunion, G. L. Kane and J. Wudka, Nucl. Phys. B **299**, 231 (1988); J. F. Gunion and L. H. Orr, Phys. Rev. D **46**, 2052 (1992); J. F. Gunion and T. Han, Phys. Rev. D **51**, 1051 (1995); R. Kinnunen, S. Lehti, A. Nikitenko and P. Salmi, J. Phys. G **31**, 71 (2005); J. Dai, J. F. Gunion and R. Vega, Phys. Lett. B **345**, 29 (1995); D. Froidevaux and E. Richter-Was, Z. Phys. C **67**, 213 (1995); M. S. Carena, S. Mrenna and C. E. M. Wagner, Phys. Rev. D **62**, 055008 (2000); C. Balazs, J. L. Diaz-Cruz, H. J. He, T. M. P. Tait and C. P. Yuan, Phys. Rev. D **59**, 055016 (1999); J. L. Diaz-Cruz, H. J. He, T. M. P. Tait and C. P. Yuan, Phys. Rev. Lett. **80**, 4641 (1998); H. S. Hou, W. G. Ma, R. Y. Zhang, Y. B. Sun and P. Wu, JHEP **0309**, 074 (2003); J. j. Cao, G. p. Gao, R. J. Oakes and J. M. Yang, Phys. Rev. D **68**, 075012 (2003); C. Kao and N. Stepanov, Phys. Rev. D **52**, 5025 (1995); A. Belyaev, M. Drees, O. J. P. Eboli, J. K. Mizukoshi and S. F. Novaes, Phys. Rev. D **60**, 075008 (1999); G. Cynolter, E. Lendvai and G. Pocsik, Acta Phys. Polon. B **31**, 1749 (2000); E. Boos, A. Djouadi and A. Nikitenko, Phys. Lett. B **578**, 384 (2004); A. Djouadi, W. Kilian, M. Muhlleitner and P. M. Zerwas, Eur. Phys. J. C **10**, 45 (1999); Z. Kunszt and F. Zwirner, Nucl. Phys. B **385**, 3 (1992); T. Plehn, D. L. Rainwater and D. Zeppenfeld, Phys. Lett. B **454**, 297 (1999).
  - [3] G. Aad *et al.* [The ATLAS Collaboration], arXiv:0901.0512 [hep-ex].
  - [4] A. de Roeck, A. Ball, M. Della Negra, L. Foa, and A. Petrilli [The CMS Collaboration], CERN-LHCC-2006-021 ; CMS-TDR-008-2.
  - [5] H. Baer, M. Bisset, X. Tata and J. Woodside, Phys. Rev. D **46**, 303 (1992).
  - [6] I. Hinchliffe, F. E. Paige, M. D. Shapiro, J. Soderqvist and W. Yao, Phys. Rev. D **55**, 5520 (1997) [arXiv:hep-ph/9610544].
  - [7] A. Datta, A. Djouadi, M. Guchait and Y. Mambrini, Phys. Rev. D **65**, 015007 (2002) [arXiv:hep-ph/0107271].
  - [8] A. Datta, A. Djouadi, M. Guchait and F. Moortgat, Nucl. Phys. B **681**, 31 (2004) [arXiv:hep-ph/0303095].
  - [9] P. Bandyopadhyay, A. Datta and B. Mukhopadhyaya, Phys. Lett. B **670**, 5 (2008) [arXiv:0806.2367 [hep-ph]].
  - [10] K. Huitu, R. Kinnunen, J. Laamanen, S. Lehti, S. Roy and T. Salminen, Eur. Phys. J. C **58**, 591 (2008) [arXiv:0808.3094 [hep-ph]].
  - [11] P. Bandyopadhyay, JHEP **0907**, 102 (2009) [arXiv:0811.2537 [hep-ph]].
  - [12] A. C. Fowler and G. Weiglein, JHEP **1001**, 108 (2010) [arXiv:0909.5165 [hep-ph]].
  - [13] J. M. Butterworth, A. R. Davison, M. Rubin and G. P. Salam, Phys. Rev. Lett. **100**, 242001 (2008) [arXiv:0802.2470 [hep-ph]].
  - [14] G. D. Kribs, A. Martin, T. S. Roy *et al.*, [arXiv:0912.4731 [hep-ph]].
  - [15] J. M. Butterworth, J. R. Ellis and A. R. Raklev, JHEP **0705**, 033 (2007) [arXiv:hep-ph/0702150].
  - [16] T. Plehn, G. P. Salam and M. Spannowsky, arXiv:0910.5472 [hep-ph].
  - [17] S. P. Martin, In \*Kane, G.L. (ed.): Perspectives on supersymmetry\* 1-98. [hep-ph/9709356].
  - [18] A. Djouadi, J. L. Kneur, G. Moultaka, Phys. Rev. Lett. **80**, 1830-1833 (1998). [hep-ph/9711244].

- [19] A. Djouadi, J. L. Kneur, G. Moultaka, Nucl. Phys. **B569**, 53-81 (2000). [hep-ph/9903218].
- [20] ATLAS Collaboration, ATL-PHYS-PUB-2009-088.
- [21] K. Agashe, A. Belyaev, T. Krupovnickas, G. Perez and J. Virzi, Phys. Rev. D **77**, 015003 (2008);
- [22] M. Gerbush, T. J. Khoo, D. J. Phalen, A. Pierce and D. Tucker-Smith, Phys. Rev. D **77**, 095003 (2008); ATL-PHYS-CONF-2008-008 and ATL-COM-PHYS-2008-001, Feb. 2008
- [23] G. Brooijmans, ATL-PHYS-CONF-2008-008, ATL-COM-PHYS-2008-001, Feb 2008.
- [24] J. Thaler and L. T. Wang, JHEP **0807**, 092 (2008) [arXiv:0806.0023 [hep-ph]].
- [25] D. E. Kaplan, K. Rehermann, M. D. Schwartz and B. Tweedie, Phys. Rev. Lett. **101**, 142001 (2008) [arXiv:0806.0848 [hep-ph]].
- [26] L. G. Almeida, S. J. Lee, G. Perez, G. Sterman, I. Sung and J. Virzi, Phys. Rev. D **79**, 074017 (2009) [arXiv:0807.0234 [hep-ph]].
- [27] L. G. Almeida, S. J. Lee, G. Perez, I. Sung and J. Virzi, Phys. Rev. D **79**, 074012 (2009) [arXiv:0810.0934 [hep-ph]].
- [28] D. Krohn, J. Thaler and L. T. Wang, JHEP **0906**, 059 (2009) [arXiv:0903.0392 [hep-ph]].
- [29] S. D. Ellis, C. K. Vermilion and J. R. Walsh, Phys. Rev. D **80**, 051501 (2009) [arXiv:0903.5081 [hep-ph]].
- [30] S. D. Ellis, C. K. Vermilion and J. R. Walsh, arXiv:0912.0033 [hep-ph].
- [31] S. Chekanov and J. Proudfoot, Phys. Rev. D **81**, 114038 (2010) [arXiv:1002.3982 [hep-ph]].
- [32] T. Sjostrand, S. Mrenna and P. Skands, JHEP **0605**, 026 (2006) [arXiv:hep-ph/0603175].
- [33] G. Belanger, F. Boudjema, A. Pukhov and A. Semenov, arXiv:1005.4133 [hep-ph].
- [34] N. Arkani-Hamed, A. Delgado and G. F. Giudice, Nucl. Phys. B **741**, 108 (2006) [arXiv:hep-ph/0601041].
- [35] J. M. Butterworth, J. R. Ellis, A. R. Raklev and G. P. Salam, Phys. Rev. Lett. **103**, 241803 (2009) [arXiv:0906.0728 [hep-ph]].
- [36] D. Krohn, J. Thaler and L. T. Wang, JHEP **1002**, 084 (2010) [arXiv:0912.1342 [hep-ph]].
- [37] D. E. Soper and M. Spannowsky, arXiv:1005.0417 [hep-ph].
- [38] C. Hackstein and M. Spannowsky, arXiv:1008.2202 [hep-ph].
- [39] Y. L. Dokshitzer, G. D. Leder, S. Moretti and B. R. Webber, JHEP **9708**, 001 (1997) [arXiv:hep-ph/9707323].
- [40] M. Wobisch and T. Wengler, arXiv:hep-ph/9907280.
- [41] M. Wobisch, PhD Thesis (2000).
- [42] M. Cacciari and G. P. Salam, Phys. Lett. B **641**, 57 (2006) [arXiv:hep-ph/0512210].
- [43] A. Bassetto, M. Ciafaloni and G. Marchesini, Phys. Rept. **100**, 201 (1983).
- [44] A. Djouadi, J. L. Kneur and G. Moultaka, Comput. Phys. Commun. **176**, 426 (2007) [arXiv:hep-ph/0211331].
- [45] M. L. Mangano, M. Moretti, F. Piccinini, R. Pittau and A. D. Polosa, JHEP **0307**, 001 (2003) [arXiv:hep-ph/0206293].
- [46] C. M. Buttar, D. Clements, I. Dawson and A. Moraes, Acta Phys. Polon. B **35**, 433 (2004).
- [47] P. Nason, S. Dawson, R. K. Ellis, Nucl. Phys. **B303**, 607 (1988).
- [48] U. Aglietti, A. Belyaev, S. Berge *et al.*, [hep-ph/0612172].
- [49] R. Bernhard et al [HFAG rare decay group], <http://www.slac.stanford.edu/xorg/hfag/rare/index.html>
- [50] N. Chen, D. Feldman, Z. Liu *et al.*, Phys. Lett. **B685**, 174-181 (2010). [arXiv:0911.0217 [hep-ph]].
- [51] R. Kitano and Y. Nomura, arXiv:hep-ph/0606134.